Journal of Power Sources 193 (2009) 17–23

Contents lists available at ScienceDirect

Journal of Power Sources

journal homepage: www.elsevier.com/locate/jpowsour

Effect of Pd loading in Pd-Pt bimetallic catalysts doped into hollow core mesoporous shell carbon on performance of proton exchange membrane fuel cells

Berker Fıçıcılar[a], Ayşe Bayrakçeken[b], İnci Eroğlu[a,*]

[a] Department of Chemical Engineering, Middle East Technical University, Ankara 06531, Turkey
[b] Department of Chemical Engineering, Atatürk University, Erzurum 25240, Turkey

ARTICLE INFO

Article history:
Received 3 November 2008
Received in revised form
28 December 2008
Accepted 24 January 2009
Available online 10 February 2009

Keywords:
PEMFC
Palladium
Platinum
Nanoparticles
Hollow core mesoporous shell carbon
Microwave irradiation

ABSTRACT

A significantly active Pd-Pt/carbon electrocatalyst for polymer electrolyte membrane fuel cells was synthesized by microwave irradiation using a hollow core mesoporous shell (HCMS) carbon as catalyst support that was prepared by template replication of core/shell spherical silica particles and two different carbon precursors. Pt/Pd percent weight ratios on carbon support were varied as 20/0, 15/5, 10/10, 5/15 to 0/20. As the average pore diameter of the carbon support was increased from 3.02 nm to 3.90 nm by changing the type of the carbon precursor, fuel cell performances of the HCMS carbon based Pd-Pt bimetallic catalysts were improved significantly.

1. Introduction

Over the last decade, comprehensive research on the development of proton exchange membrane fuel cells (PEMFCs) resulted in significant increase in the catalytic performance of membrane electrode assemblies (MEAs). Considering efficiency and cost requirements [1], one major challenge is arising from the electrocatalytic layers of the PEMFCs. For hydrogen oxidation and oxygen reduction reactions in these electrocatalytic layers, dispersion of active metal catalysts as nanoparticles over electronically conductive carbon support is necessary to provide effective catalyst utilization. Catalytic activity of the fuel cell electrocatalysts depends on several parameters such as metal particle shape and size as well as particle size distribution, catalyst preparation technique, structure of the catalyst support, precursor properties, and accessibility of the active metal on the carbon support [2].

Platinum on carbon (Pt/C) is one of the most effectively utilized electrocatalyst for PEMFC applications [3–5]. Microstructure of the catalyst support affects the PEMFC performance. At relatively high current densities, water management issue becomes critical and multiphase transport of reactants and products dominate the performance of the fuel cell [6,7]. Carbon supported Pt nanoparticles exhibit improved fuel cell performance in comparison to unsupported platinum catalysts [8].

Carbon is chemically stable in acidic and basic media and active metal is dispersed over a high surface area carbon support. Electronically conductive properties of carbon facilitate the interaction at the electrode–electrolyte–reactant interface (three phase boundary) resulting in an increased fuel cell performance [9].

The most commonly used carbon support is Vulcan XC72 which has random pores with varying sizes that may lead to an inefficient multiphase transfer of reactants and products. Many alternative carbon materials have been synthesized [10–12]. For the properly passage of reactants and products with increased electrodics, bimodal (meso/macro) and adjustable pore structure of hollow core mesoporous shell (hereinafter, referred to as HCMS) carbon can facilitate the diffusion of hydrogen and oxygen as well as the water transport within the fuel cell [13].

For the carbon supported fuel cell catalysts, carbon–metal interactions occur and additional active metal incorporation to the supported platinum catalysts may improve the platinum–carbon configuration [14]. Bimetallic Pt-Co/C cathode catalysts improved the durability in PEMFCs by reducing Pt dissolution and migration during the course of operation [15,16]. Bimetallic Pt-Ru/C catalysts improved the carbon dioxide tolerance of PEMFCs [20]. There are several ways to deposit metal alloys over the carbon supports. Of all

* Corresponding author. Tel.: +90 312 210 2609; fax: +90 312 210 2600.
E-mail address: ieroglu@metu.edu.tr (İ. Eroğlu).

0378-7753/$ – see front matter © 2009 Elsevier B.V. All rights reserved.
doi:10.1016/j.jpowsour.2009.01.094

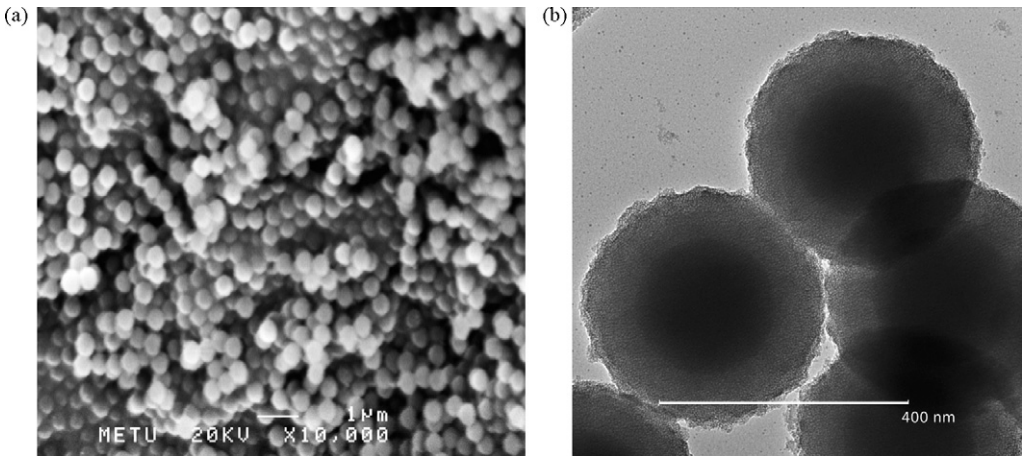

Fig. 1. SEM (a) and TEM (b) images of solid core mesoporous shell (SCMS) silica.

the other catalyst preparation techniques, microwave irradiation is gaining an increasing attention because of being energy and time efficient [17–20].

Pd is another noble metal with significant electrocatalytic activity and it is widespread in the earth crust. It is less expensive and stable in acidic solutions. In the present study, bimetallic Pd-Pt over HCMS carbon electrocatalysts is suggested to improve oxygen reduction reaction (ORR) and hydrogen oxidation reaction (HOR). In this work, it is aimed to synthesize Pd-Pt bimetallic catalysts supported with a novel HCMS carbon by microwave irradiation. HCMS carbon spheres with periodically ordered structural properties are synthesized by two different carbon precursors with the template replication of sub micrometer-size solid core mesoporous shell (SCMS) silica spheres.

2. Experimental

2.1. Solid core mesoporous shell (SCMS) silica synthesis

Monodisperse colloidal silica spheres can be prepared from tetraalkoxysilanes in alcoholic solutions. Hydrolysis and condensation of the monomers are catalyzed by ammonia and alcohol and water act as co-solvents [21,22]. Yu et al. [23] and Unger et al. [24] outlined the synthesis of SCMS silica spheres with the sol–gel polymerization of tetraethoxysilane (TEOS) and octadecyltrimethoxysilane (C18TMS).

SCMS silica is synthesized with the addition of 3.5 ml of aqueous ammonia (28–30%, ACROS) into a solution containing 74 ml of ethanol (99.8%, Riedel-de Haën) and 10 ml of deionized water. This mixture was heated up to 303 K and then 6 ml of TEOS (98%, ACROS) was added rapidly into the mixture as silica source under vigorous stirring and the reaction mixture was kept stirred for 1 h to yield uniform silica spheres. A mixture containing 5 ml of TEOS and 2 ml C18TMS (tech. 90%, Aldrich) was added drop wise over a 15 min period into the colloidal solution containing silica spheres and mixture was further reacted for 1 h. The resulting material was retrieved by centrifugation until the pH of the solution was stabilized. Nanocomposite material was dried in vacuum oven at 353 K and removal of the organic group from the octadecyltrimethoxy-incorporated silica was achieved by calcination in a tubular furnace at 803 K for 6 h under oxygen atmosphere.

2.2. Hollow core mesoporous shell (HCMS) carbon synthesis

SCMS silica is used as a template for further polymerization and carbonization steps for the synthesis of HCMS carbon [23]. In order to form acidic catalytic sites for phenolic resin polymerization reaction, aluminum was incorporated into the silicate framework via an impregnation method. For the impregnation of aluminum on SCMS silica, 1 g of SCMS silica was added to an aqueous solution containing 0.3 g of $AlCl_3{\cdot}6H_2O$ (99.0%, Fluka) in 0.35 ml of deionized water. The resulting slurry was stirred for 1 h. The powder was dried in air at 353 K. Finally, the Al-impregnated SCMS silica was calcined at 803 K for 5 h in air to obtain the SCMS-aluminosilicate nanocomposite material.

For phenol/resin formation as carbon precursor over the aluminosilicate framework, 0.38 g of phenol per gram of the SCMS-aluminosilicate template was incorporated into the mesopores by heating at 373 K for 12 h under vacuum. The resulting phenol-incorporated SCMS aluminosilicate was reacted with 0.25 g paraformaldehyde under vacuum at 403 K for 24 h to yield phenolic resin/HCMS-aluminosilicate nanocomposite inside the mesopores.

The phenol-resin incorporated nanocomposite material was heated with a ramp of 1 K min^{-1} to 433 K and held at that temperature for 5 h under the flowing nitrogen. The temperature was then ramped at 5 K min^{-1} to 1103 K and held at this temperature for 8 h to carbonize the phenolic resin inside the mesopores of HCMS aluminosilicate to obtain carbon/aluminosilicate nanocomposite. The aluminosilicate template was dissolved by using 48% HF solution resulted in hollow core mesoporous shell carbon (hereinafter, referred to as HCMS1) obtained from the phenolic resin route.

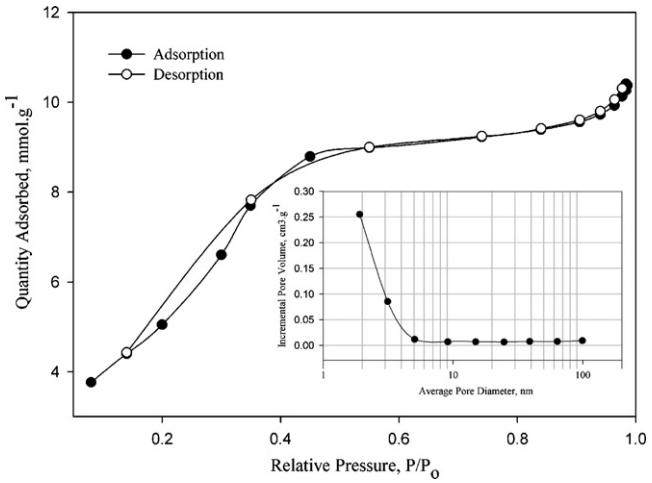

Fig. 2. N_2 adsorption/desorption isotherms and the corresponding pore size distribution for SCMS silica.

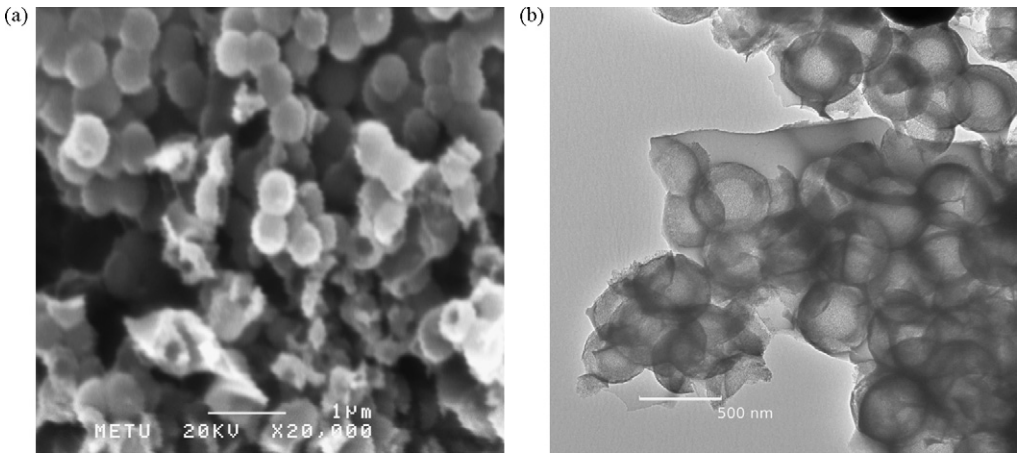

Fig. 3. SEM (a) and TEM (b) images of hollow core mesoporous shell (HCMS) carbon.

In case of using divinylbenzene (DVB) as carbon precursor, SCMS silica was first dehydrated overnight at 473 K under vacuum. After that a carbon precursor solution containing 2 ml DVB for 1 g SCMS silica and AIBN (DVB/AIBN molar ratio is approximately 24) is added to the mesopores of SCMS silica template. The mixture is placed into a 25 ml Schlenk tube. Three freeze-pump-thaw cycles are performed to remove the dissolved oxygen. Polymerization is conducted at 343 K for 18 h under nitrogen atmosphere in a drying oven. Resultant composite material is carbonized at 1103 K for 8 h with a ramp of 1 K min^{-1} under nitrogen flow. Etching of the silica template with 48% HF from the calcined nanocomposite material yields the hollow core mesoporous shell carbon (hereinafter, referred to as HCMS2).

2.3. Catalyst preparation

HCMSs prepared by different routes (HCMS1 and HCMS2) were used as the catalyst support material. As platinum and palladium precursors hexachloroplatinic acid (H_2PtCl_6, ca. 40% Pt ACROS) and palladium (II) chloride ($PdCl_2$, 99.9% Aldrich) were used. In the catalyst preparation, a microwave oven (Akai, 2450 MHz, and 800 W) was used. The commercial Pt (20% Pt/C, ETEK®) catalyst was selected for comparison. The prepared and commercial catalysts were used as either anode or cathode electrodes. Pd ratio in the carbon supported bimetallic Pd-Pt catalysts were varied between 0 and 20%.

Pt/HCMS catalysts were prepared by using microwave heating of ethylene glycol solutions of the metal precursors [19]. Briefly, 0.05 M aqueous solutions of Pt and Pd precursors were prepared. A required volume of these solutions which corresponds to the desired Pt and Pd loadings were mixed with 50 ml ethylene glycol (EG) in a 100 ml beaker. Then, 0.1 g HCMS carbon was added to the solution. After ultrasonic mixing for half an hour, the mixture was put in the center of the microwave oven and heated for 120 s by means of an 800 W microwave power. The resulting suspension was cooled immediately, and then filtered off and the residue was washed with acetone and deionized water. The solid product was dried overnight at 373 K in a vacuum oven [20].

2.4. Catalyst characterization

N_2 adsorption analysis was performed with a surface area analyzer (Micromeritics Gemini V 2365) to determine the structural properties of the catalysts. The crystalline structures of supported Pd-Pt/HCMS electrocatalysts were characterized by measuring their X-ray diffraction (XRD) patterns on a Rigaku Ultima D-Max 2200 with monochromatic Cu Kα radiation. The scanning range of 2θ was set between 5° and 85° with a step size of 0.02°. Additional ex situ characterization of the catalytic materials was performed with X-ray photoelectron spectroscopy (XPS, Specs GMBH), scanning electron microscopy (SEM, Quanta FEG), and transmission electron microscopy (TEM, JEOL 2100F) measurements.

2.5. PEMFC performance tests

The MEA preparation method is given elsewhere [25]. Briefly, the prepared catalyst ink sprayed onto the gas diffusion layers and then hot pressed onto the Nafion® 112 membrane. After the construction of the single cell by using a commercial hardware (Electrochem, FC05-01 SP REF), the fuel cell tests were performed by using the home made fuel cell test station [25].

Performance tests were conducted at ambient pressure and fuel cell temperature was set to 70 °C, whereas anode and cathode humidifiers were adjusted to 70 °C. All lines prior to fuel cell were heated to maintain the uniform temperature at the inlet to the fuel cell. Pure hydrogen and oxygen gases are used as reactants and both of the reactants fixed flow rate were kept at 100 cm^3 min^{-1} during the experiments.

Fuel cell is first purged with nitrogen for 30 min and then operated at 0.5 V for several hours. Potentiostatic measurements were carried out with an electronic load (TDI dynaload RBL488 400 W) integrated to the single fuel cell. Steady state currents are recorded for adjusted potentials.

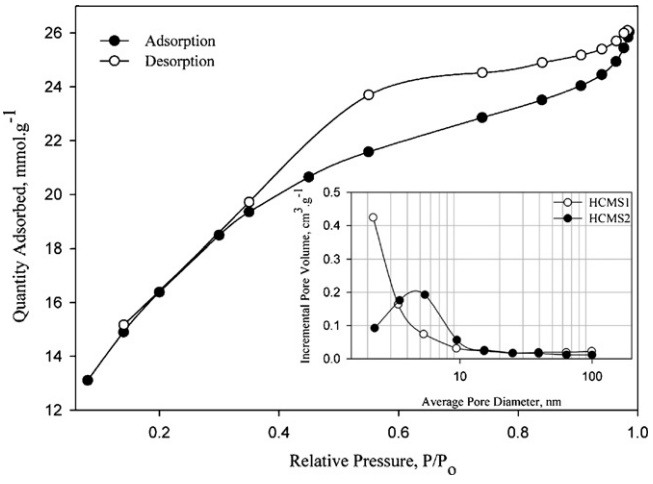

Fig. 4. N_2 adsorption/desorption isotherms and the corresponding pore size distribution for HCMS carbon.

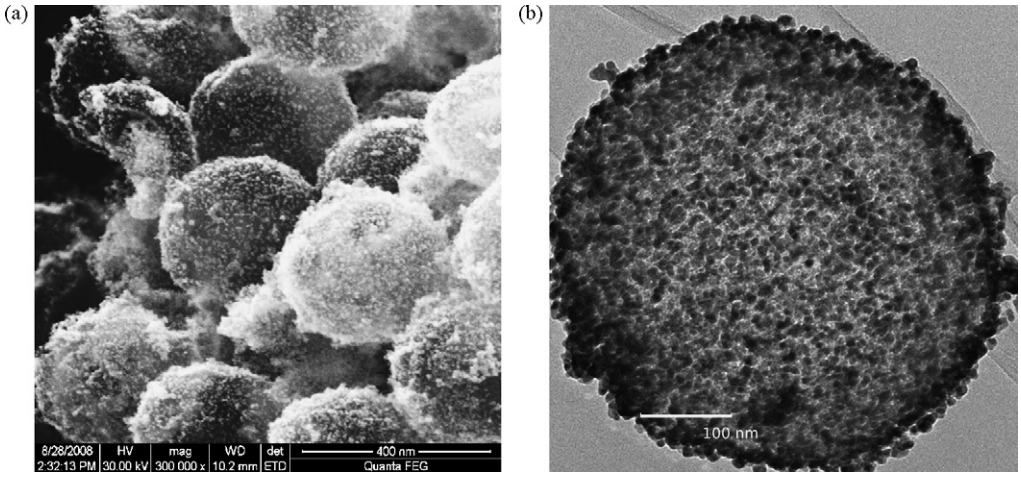

Fig. 5. SEM (a) and TEM (b) micrograph of 20% Pt/HCMS2.

3. Results and discussion

3.1. Solid core mesoporous shell silica

Sub micrometer-size silica spheres exhibiting solid core mesoporous shell structure were synthesized with a molar ratio of TEOS/C18TMS = 5.3 [23,24]. Adjusting the molar ratio of TEOS/C18TMS, one can change the core and the shell thicknesses of the silica template [26]. Scanning electron microscopy (SEM) images of SCMS silica spheres (Fig. 1a) showed that the spheres are uniformly distributed with an average particle size of 490 nm. The transmission electron microscopy (TEM) micrograph of the SCMS silica (Fig. 1b) indicates the formation of spherical particles with a core diameter of 300 nm and shell thickness of 95 nm.

Typical nitrogen adsorption/desorption isotherms and corresponding pore size distribution for SCMS silica are shown in Fig. 2. Brauner-Emett-Teller (BET) surface area of SCMS silica was calculated as 492 $m^2\,g^{-1}$ for a total pore volume of 0.40 $cm^3\,g^{-1}$. The pore size distribution data calculated from the adsorption branches of nitrogen isotherms by the Barrett-Joyner-Halenda (BJH) method indicated that the pores of the SCMS silica template are uniform and centered at 2.41 nm.

3.2. Hollow core mesoporous shell carbon

Characterization of the spherical hollow core mesoporous shell carbon structures was conducted with nitrogen adsorption, SEM and TEM analysis. SEM micrograph of HCMS carbon (Fig. 3a) revealed that spherical carbons were uniformly distributed with an average particle diameter of 500 nm and some carbon capsules were fragmented. TEM image (Fig. 3b) of the HCMS carbon particles exhibited a uniform particle size with a core diameter of 340 nm and shell thickness of 80 nm, respectively.

HCMS1 nitrogen adsorption/desorption isotherms at 77 K and corresponding pore size distributions for HCMS1 and HCMS2 are shown in Fig. 4. The isotherm for HCMS carbon exhibited type IV isotherm with a H2 hysteresis (according to IUPAC classification). The pore size distribution of the prepared HCMS carbon spheres is uniform and the average pore diameter is 3.02 nm for HCMS1 and 3.90 nm for HCMS2 estimated from BJH analysis for the adsorption branches of the isotherm data. BET surface area of HCMS carbon was found as 1290 $m^2\,g^{-1}$ for HCMS1 and 759 $m^2\,g^{-1}$ for HCMS2. BET surface areas for the prepared Pt-Pd/HCMS2 catalysts are given in Table 1.

3.3. Characterization of Pd-Pt/HCMS electrocatalysts

Fig. 5 shows SEM and TEM images of Pt/HCMS2 electrocatalyst. It is clearly seen from the TEM image that Pt nanoparticles were uniformly distributed over carbon support. However, some of the spheres were corrupted and particle growth for some specific regions was observed.

Fig. 6a shows the XRD patterns of the SCMS silica template and HCMS2 carbon and Fig. 6b shows the typical XRD patterns of Pt-Pd/HCMS2 for different Pt/Pd percent weight ratios on carbon support. The XRD pattern for the SCMS silica particles as shown in Fig. 6a, indicated a strong primary (1 0 0) diffraction peak centered at $2\theta = 2.10^\circ$. A slight shift to lower angles was detected related to the alkyl chain length of the surfactant [27]. The XRD pattern of the HCMS2 carbon spheres revealed a strong (0 0 2) diffraction peak centered at $2\theta = 18^\circ$, demonstrating the amorphous character of the carbon [26]. From Fig. 6b, it is observed that all the XRD patterns of the Pt-Pd/HCMS2 catalysts exhibit the main characteristic peaks of fcc crystalline Pt and Pd with the planes of (1 1 1), (2 0 0), (2 2 0) and (3 1 1). The particle sizes of the catalysts were calculated by using Scherrer equation for the half-full-width at half maximum of the (2 2 0) inflection and given in Table 2. As can be seen from the table, for the Pt/HCMS2 catalyst the particle size was calculated as 4 nm. With the addition of the second metal of Pd, the particle sizes of the bimetallic catalysts increased. The diffraction peaks were slightly shifted to higher 2θ values for the bimetallic and also for Pd/HCMS2 catalysts when compared to Pt/HCMS2 catalyst.

Table 1
BET surface areas for the prepared catalysts.

Catalyst	Pt (%)	Pd (%)	BET surface area ($m^2\,g^{-1}$)	Total volume ($cm^3\,g^{-1}$)
Pt/HCMS2	20	0	277	0.33
PtPd/HCMS2	15	5	325	0.41
PtPd/HCMS2	10	10	262	0.34
PtPd/HCMS2	5	15	319	0.39
Pd/HCMS2	0	20	335	0.41

Table 2
Particle sizes calculated for the prepared Pd-Pt/HCMS2 catalysts by using the XRD patterns.

Catalyst	Pt (%)	Pd (%)	Particle size (nm)
Pt/HCMS2	20	0	4
PtPd/HCMS2	15	5	5
PtPd/HCMS2	10	10	8
PtPd/HCMS2	5	15	6
Pd/HCMS2	0	20	16

Table 3
Current and power densities for the prepared catalysts at 0.6 V and 0.4 V.

Catalyst	@0.6 V		@0.4 V	
	Current density (mA cm^{-2})	Power density (W cm^{-2})	Current density (mA cm^{-2})	Power density (W cm^{-2})
Pt/HCMS1	233	0.14	451	0.18
PtPd/HCMS1 (15:5)	265	0.16	531	0.21
PtPd/HCMS1 (10:10)	100	0.06	343	0.14
PtPd/HCMS1 (5:15)	143	0.08	335	0.13
Pd/HCMS1	28	0.02	215	0.09
Pt/HCMS2	329	0.20	560	0.22
PtPd/HCMS2 (15:5)	250	0.15	480	0.19
PtPd/HCMS2 (10:10)	164	0.10	349	0.14
PtPd/HCMS2 (5:15)	138	0.08	472	0.19
Pd/HCMS2	98	0.06	237	0.10
Pt/C (ETEK)[20]	524	0.31	808	0.32

Fig. 7 shows the XPS spectra for Pt 4f core level spectra. The two doublets for high and low energy bands are seen at around 71.3 eV and 74.5 eV which correspond to Pt4f$_{7/2}$ and Pt4f$_{5/2}$, respectively, indicating the existence of Pt metal. Also the Pd 3d core level spectrum is given in Fig. 8. The two doublets corresponding to Pd 3d were seen at around 335.3 eV and 340.5 eV which correspond to Pd 3d$_{5/2}$ and Pd 3d$_{3/2}$, respectively, indicating the existence of Pd metal. The shift of the peaks is shown with dashed lines in the figures which might be resulted from the alloy formation and the electronic interaction between Pt and Pd atomic orbit [28]. The survey spectra for Pt/HCMS2, PtPd/HCMS2 (10:10) and Pd/HCMS2 are given in Fig. 9. As can be seen from the figure carbon and oxygen peaks exist for all catalysts. C1 s peak was observed at a binding energy of 284.4 eV, whereas O1 s binding energy values were centered at 532.0–532.8 eV. The oxidation states information of the elements composed of Pt-Pd/HCMS2 materials was obtained by XPS studies. Amount of oxygenated groups on the carbon support affects the platinum and palladium surface areas. Interaction of platinum with the carbon support shifts the peak maxima from the expected 70.9 eV value to the higher values of 71.3 eV and 71.2 eV for the catalysts Pt/HCMS2 and Pt-Pd/HCMS2 (10:10), respectively. Shift of Pt4f$_{7/2}$ core level spectra can be considered as a measurement of oxidized platinum [29]. Palladium surface oxidation is character-

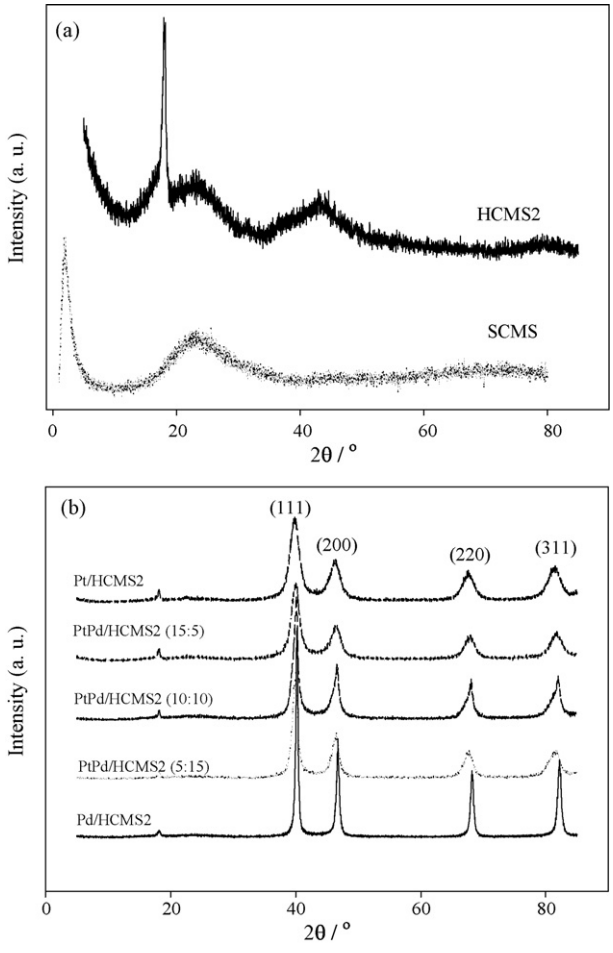

Fig. 6. The XRD patterns of (a) as-synthesized SCMS silica and HCMS2 carbon, and (b) Pt-Pd/HCMS2 catalysts.

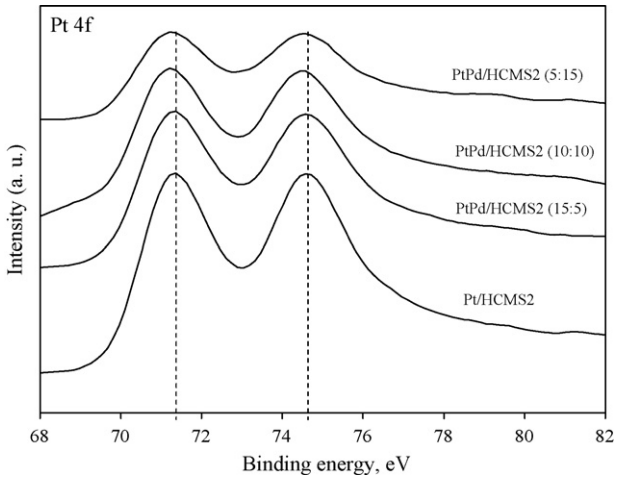

Fig. 7. Pt 4f XPS spectra for HCMS2 based catalysts.

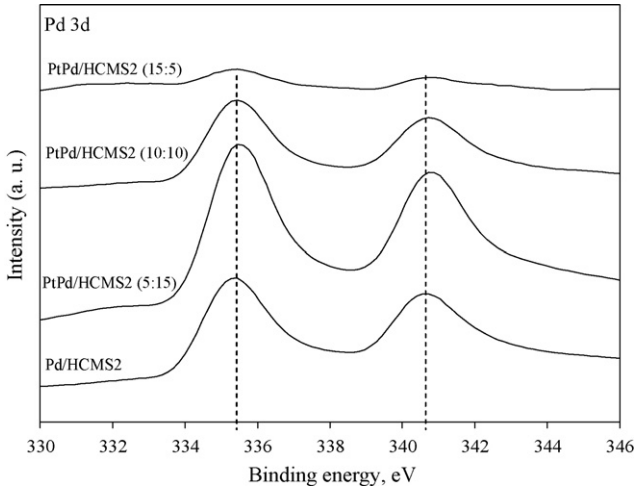

Fig. 8. Pd 3d XPS spectra for HCMS2 based catalysts.

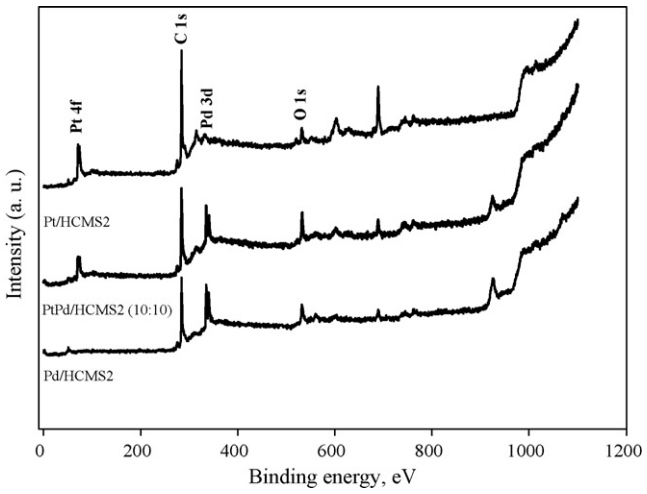

Fig. 9. XPS survey spectra for Pt/HCMS2, PtPd/HCMS2 (10:10) and Pd/HCMS2.

ized by Pd $3d_{5/2}$ peaks at 334.9 eV, 335.5 eV, and 336.3 eV, which corresponds to the bulk Pd atoms and Pd atoms with two and four O neighbors, respectively. XPS survey spectra given in Fig. 9, indicates Pd $3d_{5/2}$ peaks centered at 335.2 eV. This slight shift might signify the oxidation of Pd atoms with two O neighbors [30].

Surface elemental composition was obtained by XPS analysis. Despite the presence of contaminants in the electrocatalysts, the XPS spectra were all dominated by palladium, platinum, and carbon signals. During the synthesis, extraneous anions like F^- and Cl^- were detected due to the use of HF in the etching process and metal precursors (H_2PtCl_6, $PdCl_2$) to incorporate palladium and platinum, respectively. Even though the presence of extraneous anions in small amounts in the electrocatalysts, no detrimental effect on fuel cell performance was observed.

3.4. PEMFC performance tests

Fig. 10 shows the PEMFC polarization curve of the HCMS1 based catalysts. The curve shows that only the addition of 5% Pd into Pt/HCMS1 catalyst increased the performance of the PEMFC. The best fuel cell performance was observed for Pd-Pt/HCMS1 containing 5% Pd and 15% Pt. Additional increase of palladium content lowered the fuel cell performance when HCMS1 was used as catalyst support. At high current densities (>300 mA cm^{-2}) the difference between the fuel cell performances of Pt-Pd/HCMS1 (5:15) and PtPd/HCMS1 (10:10) catalysts decreased and similar results

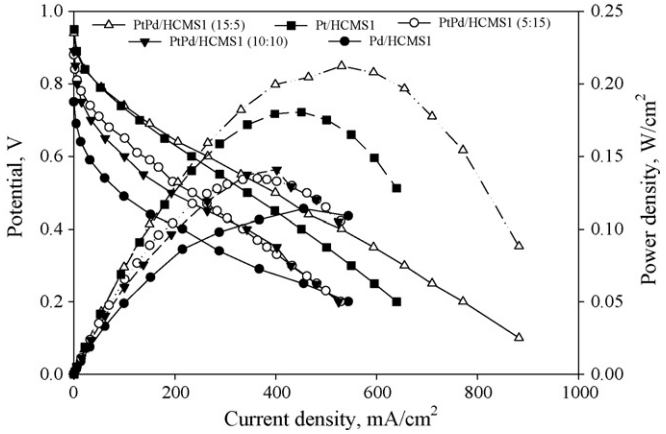

Fig. 10. PEMFC polarization curve of the HCMS1 based cathode catalysts (anode catalyst is 20% Pt/C, ETEK).

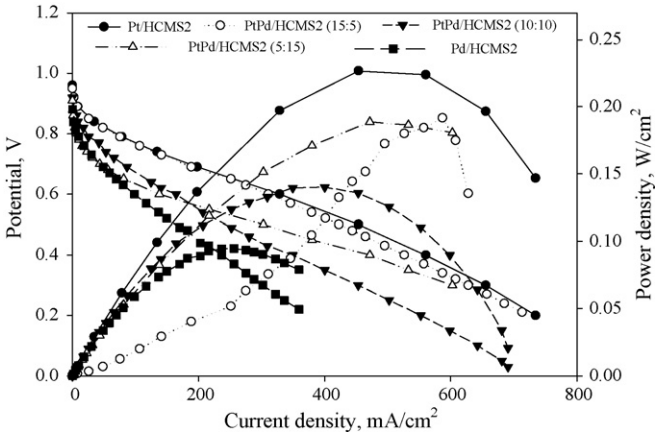

Fig. 11. PEMFC polarization curve of the HCMS2 based cathode catalysts (anode catalyst is 20% Pt/C, ETEK).

were obtained. The current and power densities of the catalysts at 0.6 V and 0.4 V potentials are given in Table 3. These results are also compared with the performance of commercial Pt/C (20%, ETEK) catalyst [20]. It should be emphasized that 5% Pd metal containing electrocatalyst has a potential to be used as cathode catalyst in further studies.

Fig. 11 shows the PEMFC performance curves of the HCMS2 based catalysts when the catalyst is used as the cathode electrode. In case of HCMS2, the best fuel cell performance was obtained with 20% Pt over HCMS2 catalyst. When compared with 20% Pt/HCMS2 catalyst, it was seen that the fuel cell performance for 5% palladium containing catalyst exhibited very close behavior to the Pt/HCMS2 electrocatalyst. Relatively lower fuel cell performances were obtained as the palladium amount was increased in the catalyst. It should be noted that Pd particle size increases with increasing Pd content. This result may indicate that Pd particle size is a critical parameter affecting the fuel cell performance.

Fig. 12 shows PEMFC performance of the HCMS2 based anode electrocatalysts. Utilization of Pd as an anode catalyst enhanced the hydrogen oxidation reaction. As the palladium content of the electrocatalyst was increased from 5% to 15%, fuel cell performance was decreased slightly. The comparison of the current and power densities of the HCMS2 based catalysts for anode and cathode electrode at 0.6 V is given in Table 4. From the table, it is clear that when the Pd doped Pt catalysts are used as anode electrode the current density is approximately doubled. Pd-Pt/HCMS2 alloy catalysts exhibited good anode electrodics compared to the cathode electrodics.

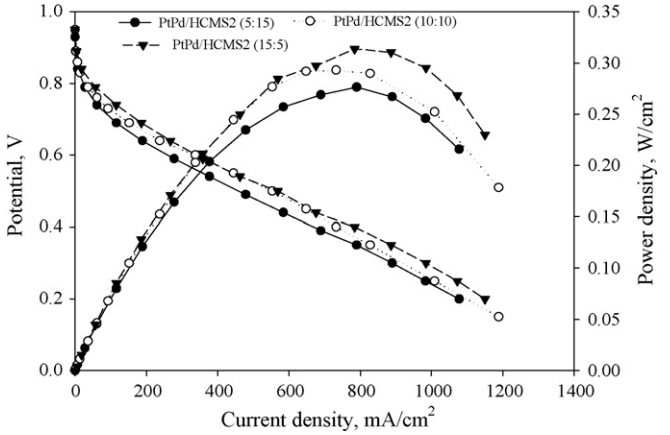

Fig. 12. PEMFC polarization curve of the HCMS2 based anode catalysts (cathode catalyst is 20% Pt/C, ETEK).

Table 4
Comparison of the current and power densities for the prepared HCMS2 based catalysts at 0.6 V either being used as anode or cathode electrode.

Catalyst	@0.6 V (as cathode)		@0.6 V (as anode)	
	Current density (mA cm^{-2})	Power density (W cm^{-2})	Current density (mA cm^{-2})	Power density (W cm^{-2})
PtPd/HCMS2 (15:5)	250	0.15	340	0.20
PtPd/HCMS2 (10:10)	164	0.10	338	0.20
PtPd/HCMS2 (5:15)	138	0.08	260	0.15

HCMS2 based electrocatalysts performed better than the HCMS1 based electrocatalysts. At relatively high current densities, transport of the reactants and the products was facilitated by increasing the average pore diameter of the hollow core mesoporous shell carbon from 3.02 nm to 3.90 nm. A further increase of average pore diameter by changing the carbon precursor or silica template structure will probably increase the fuel cell performance.

4. Conclusion

Hollow core mesoporous shell carbon was synthesized using two carbon precursors and Pd-Pt alloy catalysts over carbon supports (HCMS1 and HCMS2) were prepared by microwave irradiation method. It was concluded that as the pore size of the carbon was increased by changing the type of the carbon precursor, fuel cell performances of the HCMS2 based catalysts were improved significantly.

Pd-Pt/HCMS electrocatalysts are promising anode and cathode PEMFC catalysts. Fuel cell tests showed that Pd-Pt/HCMS2 catalysts were more active when the catalysts were used as anode electrode and the fuel cell performance was doubled. Considering the high cost and lack of reserves of platinum, palladium seems to be a promising electrocatalyst for PEMFCs.

Bimetallic catalysts exhibited a considerable activity for low Pd content Pd-Pt/HCMS catalysts. Adding Pd in small amounts might increase the stability of the electrocatalyst and can help to the reconfiguration of Pt–C interaction. An increase in the particle size of the Pd-Pt bimetallic catalysts was observed as the Pd loading was increased. Decreasing Pd-Pt alloy particle size by controlling synthesis conditions, one will probably increase the dispersion and prevent the possible agglomeration and consequently particle growth might be controlled during the course of fuel cell operation.

Acknowledgements

The authors acknowledge financial support by Turkish Scientific and Technological Research Council (TUBITAK) through grant number 104M364 and METU ÖYP project through grant number BAP-08-11-DPT2002K120510.

References

[1] E.J. Carlson, P. Kopf, J. Sinha, S. Sriramulu, Y. Yang, National Renewable Energy Laboratory, NREL/SR-560-39104, Cambridge, Massachusetts, 2005.
[2] Z. Liu, X.Y. Ling, X. Su, J.Y. Lee, J. Phys. Chem. B 108 (2004) 8234–8240.
[3] J.K. Norskov, J. Rossmeisl, A. Logadattir, L. Lindqvist, J.R. Kitchin, T. Bligaard, H. Jonsson, J. Phys. Chem. B 108 (2004) 17886–17892.
[4] M.H. Shao, T. Huang, P. Liu, J. Zhang, K. Sasaki, M.B. Vukmirovic, R.R. Adzic, Langmuir 22 (2006) 10409–10415.
[5] K. Lee, O. Savadogo, A. Ishibara, S. Mitsushima, N. Kamiya, K. Ota, J. Electrochem. Soc. 153 (2006) A20–A24.
[6] T.R. Ralph, M.P. Hogarth, Platinum Met. Rev. 46 (2002) 117–135.
[7] T.R. Ralph, M.P. Hogarth, Platinum Met. Rev. 46 (2002) 3–14.
[8] T. Van Nguyen, S. Wiley, M.V. Nguyen, in: Pre-Print Archive—American Institute of Chemical Engineering (spring national Meeting), New Orleans, LA, United States, March 11–14, 2002.
[9] A.L. Dicks, J. Power Sources 156 (2006) 128–141.
[10] F. Gloaguen, J.-M. Léger, C. Lamy, J. Appl. Electrochem. 27 (1997) 1052–1060.
[11] J. Marie, S. Berthon-Fabry, P. Achard, M. Chatenet, A. Pradourat, E. Chainet, J. Non-Cryst. Solids 350 (2004) 88–96.
[12] B.M. Babić, Lj.M. Vračar, V. Radmilović, N.V. Krstajić, Electrochim. Acta 51 (2006) 3820–3826.
[13] G. Chai, S.B. Yoon, S. Kang, J.-H. Choi, Y.-E. Sung, Y.-S. Ahn, H.-S. Kim, J.-S. Yu, Electrochim. Acta 50 (2004) 823–826.
[14] E. Antolini, L. Giorgi, F. Cardellini, E. Passalcqua, J. Solid State Electrochem. 5 (2001) 131–140.
[15] P. Yu, M. Pemberton, P. Plasse, J. Power Sources 144 (2005) 11–20.
[16] H.A. Gasteiger, S.S. Kocha, B. Sompalli, F.T. Wagner, Appl. Catal. B: Environ. 56 (2005) 9–35.
[17] O.C. Kappe, Angew. Chem. Int. Ed. 43 (2004) 6250–6284.
[18] Z.L. Liu, J.Y. Lee, W. Chen, M. Han, L.M. Gan, Langmuir 20 (2004) 181–189.
[19] Y. Liang, H. Zhang, H. Zhong, X. Zhu, Z. Tian, D. Xu, B. Yi, J. Catal. 238 (2006) 468–476.
[20] A. Bayrakçeken, L. Türker, İ. Eroğlu, Int. J. Hydrogen Energy 33 (2008) 7527–7537.
[21] W. Stöber, A. Fink, E. Bohn, J. Colloid Interface Sci. 26 (1968) 62–69.
[22] A. Van Blaaderen, J. Van Geest, A. Vrij, J. Colloid Interface Sci. 154 (1992) 481–501.
[23] S.B. Yoon, K. Sohn, J.Y. Kim, J.-S. Yu, T. Hyeon, Adv. Mater. 14 (2002) 19–21.
[24] G. Büchel, K.K. Unger, A. Matsumoto, K. Tsutsumi, Adv. Mater. 10 (1998) 1036–1038.
[25] A. Bayrakçeken, S. Erkan, L. Türker, İ. Eroğlu, Int. J. Hydrogen Energy 33 (2008) 165–170.
[26] M. Kim, S.B. Yoon, K. Sohn, J.Y. Kim, C.-H. Shin, T. Hyeon, J.-S. Yu, Microporous Mesoporous Mater. 63 (2003) 1–9.
[27] S.B. Yoon, J.-Y. Kim, J.H. Kim, Y.J. Park, K.R. Yoon, S.-K. Park, J.-S. Yu, J. Mater. Chem. 17 (2007) 1758–1761.
[28] Y. Xu, X. Lin, J. Power Sources 170 (2007) 13–19.
[29] P.L. Antonucci, V. Alderucci, N. Giordano, D.L. Cocke, H. Kim, J. Appl. Electrochem. 24 (1994) 58–65.
[30] G. Ketteler, D.F. Ogletree, H. Bluhm, H. Liu, E.L.D. Hebenstreit, M. Salmeron, J. Am. Chem. Soc. 127 (2005) 18269–18273.